ELSEVIER

DRAFT 00 (2019) 1–12

DRAFT

Paper draft

Electric field distribution in porous piezoelectric materials during polarization

Germán Martínez-Ayuso[a,*], Michael I. Friswell[a], Hamed Haddad Khodaparast[a], James I. Roscow[b], Christopher R. Bowen[b]

[a] *Swansea University*
College of Engineering, Bay Campus
Fabian Way, Crymlyn Burrows,
Swansea SA1 8EN, UK

[b] *University of Bath*
Department of Mechanical Engineering
Claverton Down, Bath, BA2 7AY, UK

Abstract

High piezoelectric coupling coefficients enable the harvesting of more energy or increase the sensitivity of sensors which work using the principle of piezoelectricity. These coefficients depend on the material properties, but the manufacturing process can have a significant impact on the resulting overall coefficients. During the manufacturing process, one of the main steps is the process of polarization. The degree of polarization depends on multiple factors and it can strongly influence the final piezoelectric coefficients. In this paper, a study on the electric field distribution on the sensitivity of the main piezoelectric and dielectric coefficients to the polarization process is performed, focusing on porous piezoelectric materials. Different inclusion geometries are considered, namely spherical, ellipsoidal and spheres with cracks. The electric field distribution at the micro scale within a representative volume element is modelled to determine the material polarization level using the finite element method. The results show that the electric field distribution is highly dependent on the inclusion geometries and cracks and it has a noticeable impact on the equivalent piezoelectric coefficients. These results are compared with experimental measurements from published literature. Good agreement is found between the ellipsoidal model and the experimental data.

Keywords: Finite element method, Polarization, Piezoelectricity, Homogenization, Porous Ceramics

1. Introduction

Piezoelectric energy harvesters can power small devices in places where the accessibility or environmental conditions make difficult to install electric cables or batteries. Using the piezoelectric effect, many authors have developed different concepts of harvesters, aiming to optimise the power output through different strategies. An extensive review on piezoelectric energy harvesting can be found in references [1] and [2]. In these review papers, the principle of the piezoelectric effect applied to energy harvesting is detailed carefully and multiple applications are highlighted. The performance of these energy harvesters depend on many factors, such as geometry or working principle, but the material properties are common to all harvester models and significantly affect the optimal performance is one of the most important factors to consider in order to optimize them. The piezoelectric material properties are defined by three tensors, the compliance tensor ($\mathbf{s}^{\mathbf{E}}$), the piezoelectric tensor ($\mathbf{d}$) and the dielectric tensor ($\boldsymbol{\epsilon}^{\boldsymbol{T}}$). The super index $(\bullet)^{\mathbf{T}}$ and $(\bullet)^{\mathbf{E}}$ indicates the parameter is measured at constant stress and at constant electric field respectively. The compliance tensor is the resistance of the material to experience strains ($\mathbf{S}$) under applied stresses ($\mathbf{T}$) and the dielectric tensor is the ability to generate electrical displacement ($\mathbf{D}$) under applied electrical field ($\mathbf{E}$). The piezoelectric tensor relates the strain

*Corresponding author
Email address: 841238@swansea.ac.uk (Germán Martínez-Ayuso)

and the electrical field using the following equations:

$$\begin{cases} \mathbf{S} &= \mathbf{s^E}\,\mathbf{T} + \mathbf{d^t}\,\mathbf{E} \\ \mathbf{D} &= \mathbf{d}\,\mathbf{T} + \boldsymbol{\epsilon}^{\boldsymbol{T}}\,\mathbf{E} \end{cases} \tag{1}$$

In energy harvesting applications, high piezoelectric coefficients and low dielectric coefficients are desirable in order to magnify the energy converted and reduce the energy losses. Thus, the use of porous piezoelectric materials is an interesting option due to its ability to vary its material coefficients by grading the porosity which could potentially improve the harvested energy through an efficient distribution of the material [3]. The porosity ($\mathcal{P}$) is defined as the volume of inclusions with respect to the total volume of inclusions and matrix material. Porosity in piezoelectric materials has already been highlighted as a beneficial characteristic for different applications such as hydrophone sensors [4, 5], energy harvesting [3, 6, 7, 8, 9] or microelectronic devices due to their good tunable characteristics [10, 11]. In porous piezoelectric materials, there is a decrease in all material coefficients but at different rates due to the porosity [12]. The porosity has an interesting effect on the d_{33} piezoelectric coefficient which is the material coefficient which relates the electric field generated and strain when both are applied in the poling direction. This parameter remains almost constant for moderate volume fractions of inclusions where there is a relatively large decrease in permittivity, and therefore the porous materials present advantageous characteristics for sensors or energy harvesting applications which require high ratios coupling coefficients. This has been interpreted by some authors [6] as an effect of the incomplete polarization of the material. This cannot always be counteracted by increasing the poling electric field because of the electrical breakdown risk. Therefore studying the distribution of the poling electric field is important in order to optimise the porous ceramic material coefficients.

In order to predict accurately the material properties of these composite materials, all possible factors should be considered carefully and included in the modelling process, for example the manufacturing process. One of the most important processes in the manufacturing is the poling. This consists of applying an electric field to a ferroelectric material in order to align the domains in the same direction. Before polarization, ferroelectric ceramics show no macroscopic piezoelectric effect due to random orientation of its microscopic domains. The applied poling electric field aligns the domains where the electric field reaches a specific value known as the coercive field. Although the coercive field is an intrinsic property of each material, the polarization is affected also by the porous composite structure, since the distribution of composite phases alters how the applied electric field distributes inside the composite [13]. When an electric field is applied to a non-conductive (dielectric) material, it generates a separation of electric charges and hence an electric field. This electric field is called the polarization electric field and is different inside

(a)

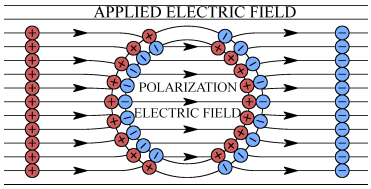

Figure 1: Polarization electric field and electric field distortion due to the inter-phase change. Polarization electric field concept. In red the positive charges and in blue the negative charges distribution around the pore.

the inclusion and outside the inclusion. Inside the inclusion this electric field is parallel and it has the same direction as the applied external electric field. Outside the inclusion, the polarization field opposes the applied electric field (Figure 1a) The polarization mechanism is discussed more detailed in references [14, 15, 16, 17]. In the case of composite materials made with inclusions with low permittivity such as air, the electric field tends to concentrate inside of these inclusions due to the lower values of permittivity [18]. Highly porous materials are therefore more difficult to polarize than dense ceramics due to the complex electric field distribution generated by the presence of inclusions [19]. In Galassi [20] the manufacturing of porous piezoelectric materials is reviewed for different techniques which are divided into two groups, dry and wet techniques. Among the dry methods, the BUrn Out Polymer Spheres (BURPS) method is the main method and free-casting is the main wet method. The BURPS method is one of the most used for fabrication of porous piezoelectric ceramics because it gives good control of the final porosity percentage and its scalability. The pore morphology can be changed by using different pore forming agent [21]. In this method, the piezoelectric material powder (PZT or $BaTiO_3$) is mixed in different proportions by weight and are uniaxially pressed to form disks. The pore forming agent is then burnt off during sintering to leave a porous structure. More information about this fabrication method can be found in reference [12, 19, 21, 22]. In Khachaturyan et al. [19] the polarization-switch mechanism and pore size are studied. The influence of isometric and anisometric pores is also studied. In both cases, the pore size was found to be irrelevant for the polarization switching mechanism, based on electric field distributions.

Many authors have studied how the electric field distribution affects the equivalent dielectric permittivity, but few have accounted for the piezoelectric coefficients in their studies. Lewis et al. [23] showed that the distribution of the poled and un-poled material inside the piezoelectric matrix considerably affects the equivalent piezoelectric coefficients. A random distribution of poled and unpoled materials is studied, and the detailed inclusion geometry was not considered, focusing more on the macro behaviour. Roscow et al. [6] also studied the piezoelectric coefficient d_{31} behaviour in order to improve the material performance. Stanculescu et al. [24] mention that

the anisotropy of pores increases with the porosity percentage, therefore, it is expected that the pore shape will deform at high porosity levels. This anisotropy in the pore shapes leads to decreases in the elastic, piezoelectric and dielectric constants [25]. Some cracks can also appear in the porous piezoelectric materials as reference [26] shows. These cracks are commonly observed for high porosity materials (more than 50% porosity) and they appear in the perpendicular direction to the die pressing direction [27]. It is also mentioned they have an important effect for high porosity, contributing to the decrease in the dielectric coefficient. These cracks might also decrease the piezoelectric coefficients by decreasing the connectivity inside the matrix or reducing the transfer of stresses.

The simulation of this decrease provoked by cracks or pore anisotropy remains a challenge which should be addressed in order to obtain accurate models to predict the material properties. In addition, accurate models of the electric field distribution might help to decide the value of the polarization field in porous piezoelectric materials. For dense materials, the applied electric field should be high enough to polarize the maximum amount of the material, but lower than the electric breakdown strength field. However, in porous piezoelectric materials this value is severely affected by the porosity, being reduced up to 70% in some cases [28]. With this uncertainty in the upper limit of the applied electric field and the uncertain distribution of porosity inside the material, the correct application of the electric field is a key factor in the manufacturing of porous material.

In this paper, a study of the sensitivity of the main piezoelectric and dielectric coefficients to the polarization process is performed for porous piezoelectric materials. A finite element cell model for polarization of porous materials is presented. The electric field distribution around spherical inclusions inside the piezoelectric matrix is considered in this model. Appropriate boundary conditions are enforced in order to simulate the cell being embedded in a periodic matrix of cells using periodic boundary conditions. This model presents a good agreement with experimental results presented in the literature. These experimental results are obtained from measurements of the material coefficients of samples manufactured in the laboratory which data has been published in references [12, 22]. The model is extended later to account for two possible cases discussed in the literature, which are: the presence of anisotropy in the pore shapes and the presence of cracks. The first case considers the presence of anisotropy in the pores for high percentages of porosity as mentioned in reference [24]. This anisotropy is studied using ellipsoidal inclusions with different geometries, but always aligned perpendicular to the poling electric field, which is the most common orientation [29]. For the second case, the presence of cracks are considered. Cracks might appear at high porosity ranges as stated in references [12, 26]. Representing cracks is difficult since cracks depend on a high number of variables, some of them with an uncertain nature such as porous distributions, imperfections, presence of contaminants, etc. Therefore, in this paper, only simple crack geometries are considered which follows the crack models described in reference [26]. These models are compared with the same experimental data in order to discuss the possible presence of anisotropy in the pore shapes or cracks. The samples presented in references [12, 22], and used in this paper, have a low degree of pore anisotropy as shown in scanning electron microscopy (SEM) pictures from the references, but it will be shown that considering low anisotropy in the pore shapes improves the agreement with respect to the experimental data. In addition, in these samples, the presence of cracks has not been reported by inspecting the lower percentages (0-30% percentages of porosity per volume) using SEM [12], and it will be shown that simple crack geometries cannot improve the matching between the experimental data and finite element model.

In this paper, the finite element modelling of the polarization process is presented in Section 2. In this section, the different geometries and homogenizations are explained, as well as the modelling of the polarization and homogenization processes. Finally, the results and discussion are presented in Section 3 and Section 4 respectively.

2. Finite Element Modelling

2.1. Representative volume modelling

Among the available homogenization techniques, the finite element (FE) method is the most appropriate technique to model the polarization process, due to its flexibility and capability to model discrete piezoelectric domains. In reference [24] the finite element method simulation is presented as an accurate method to model the permittivity of the porous materials at high porosity levels. As stated in Section 1, many authors [30, 31, 32, 33] have used FE techniques due to its flexibility and accuracy to model piezoelectric porous materials as well as its manufacturing process. The details of the computational homogenization technique can be found in [34] and hence only a brief summary is presented here.

To model composite materials in an efficient way, in statistical terms a representative volume of the composite structure has to be identified. This Representative Volume Element (RVE) has to be sufficiently small to be solvable and large enough to be representative of the structure of the composite as a whole. The choice of these RVEs depends on the geometry of the composite and the problem to address. The RVEs are composed of matrix and inclusions, and their shapes are discussed in the next sections. These RVEs are modelled using ANSYS® Finite Element package [35].

To ensure the representativeness of the RVE with respect to the material at the macro scale, appropriate boundary conditions have to be applied. Periodic boundary conditions simulate the RVE embedded in an infinite matrix of RVEs and imply that the opposite edges have identical

deformation, and opposite stress direction [36]. References [34, 37] show that these periodic boundary conditions give a good approximation of our micro-scale representative volume with respect to the macro-behaviour of the material. After applying boundary conditions to the RVE, the equivalent material parameters are calculated as explained later in Section 2.5.

2.2. Inclusion modelling

An initial model (*Model A*) which assumes perfectly spherical inclusions representing the pores is developed. This shape assumption is justified due to nature of the BURPS manufacturing process where spherical particles of pore-forming agent are burnt out when a high temperature is applied. Pore-forming agents such as polymer additives, for example, poly-ethylene oxide (PEO) [12] or poly(methyl methacrylate) (PMMA) [21] do not present high anisotropy in the pore morphology. Since in the samples used here, the additive is also a polymer, the anisotropy due to pore forming agent is neglected in this paper. Polymer additives are common in the manufacturing of piezoelectric ceramics. The authors refer to reference [38] for more information about the different additives.

To represent the geometry of this composite, a three dimensional finite element model is developed. This model contains a spherical inclusion (a pore) at the centre and one eighth of another sphere inclusion at each of the RVE corners, as Figure 2 shows. The radius of these two perfect spheres are equal and they change according to the porosity percentage, ranging from 1% to 50% of air volume respect the total volume of the RVE. This model is able to represent how the electric field distributes around the inclusions during the poling process, as Figure 2 shows, and how this electric field affects the polarization of the material elements and its distribution. These un-polarized elements (dark and light blue elements) align with the inclusions in the direction of the applied electric field. The low permittivity inclusions act as a shield avoiding the polarization of the elements, below and behind them. In our case five volumes are generated, one per inclusion. These volumes are responsible for the decrease in the material coefficients, as shown later in Section 3. For comparison purposes, another model (*model 0*) with the same geometry as model A is developed. This model has all its ferroelectric domains poled and aligned in the same direction. This model represents the theoretical maximum of the piezoelectric values.

2.3. Imperfections in the inclusion shape

During the manufacturing process, many factors might affect and lead to imperfections in the final shape of the inclusions, from excessive load during manufacturing [26], to an inappropriate selection of pore forming agent [21]. These factors might lead to anisotropy in the pore shape or even cracks, which affect the equivalent material parameters [20, 25, 26]. In reference [21] it is stated that the pore shape is affected by the pore forming agent. Different pore-forming agents generate different pore shapes.

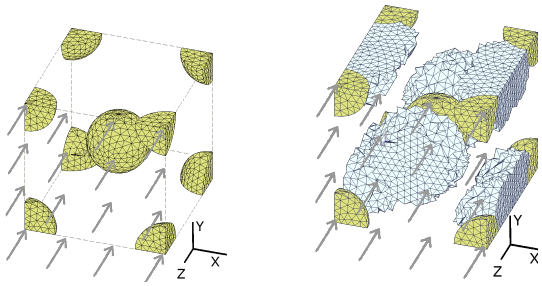

(a) (b)

Figure 2: Polarization of the model A: spherical inclusion model. The pore inclusions are shown in yellow and the poled ferroelectric elements in dark blue. The un-poled elements are shown in white and light blue to make clear the clustering of the poled piezoelectric domains around the low permittivity inclusions in the poling electrical field direction (grey arrows). a) Air inclusions in the RVE. b) Distribution of un-poled elements following the poling direction.

The pressure exerted during the die-casting on the samples might deform the pore [29]. This pressure is frequently applied in the same direction of the polarization electric field. Perpendicular to that direction, it is common for cracks to propagate in case of excessive pressure or high porosity structures [27]. Following this approach, the pore anisotropy can be regarded as the result of the deformation of the spherical inclusions in the direction of the applied load to generate oblate ellipsoids. To study this anisotropy, an ellipsoidal model is proposed (*model B*). This model contains ellipsoidal inclusions with their shorter axis aligned with the polling electric field. The other two axes remain equal and perpendicular to the applied electrical field. The geometry is presented in Figure 3 and it is composed of one ellipsoid at the centre of the RVE and one eighth of a second ellipsoidal inclusion at each corner of the RVE. Let us define the ratio between the shorter axis and any of the other two equally long axes as "aspect ratio" (τ). This parameter is used to define the ellipsoid using the following equation: $V = 4\pi(a\,b\,c)/3 = 4\pi(\tau\,a^3)$, where a,b and c are the semi-axis of the ellipsoid in the x, y and z directions. These parameters have to fulfil $a = b \neq c$ and $c = \tau\,a$. The influence of the aspect ratio is studied in this paper through a parametric study of the aspect ratio parameter. In Figure 3, the model geometry is presented for two different aspect ratio values, 0.75 and 0.35, to illustrate the model concept. No changes in the orientation of the ellipsoid are considered in this study.

To understand the effect of cracks formed during processing on the poling/piezoelectric behaviour, a crack model was developed. It should be recalled that the porosity is a key parameter in order to obtain an accurate dielectric parameter. Hence a flat crack model should be avoided. In order to meet all the requirements (flat crack with high porosity values), a modification of model A is proposed, adding a flat crack around the inclusion as Figure 4 shows. This model presents some resemblance with the cracks de-

scribed in references [26, 27], where optical micrographs of porous piezoelectric materials with a high percentage of inclusions (higher than 40%) shows the presence of cracks perpendicular to the poling direction and to the applied pressure during the manufacturing process. The authors acknowledge that a real crack will differ considerably from the proposed one. However, this model should give some insight into the possible effects of cracks in piezoelectric media. In this paper, the authors intend to obtain equivalent material properties for piezoelectric porous material after polarization, therefore, deformations or cracks which might appear during the service life are not considered. This can be extended to assume that there is no propagation of cracks (static behaviour of the cracks).

The model is intended to approximate in a simple manner the geometry of a crack keeping some key parameters equal to the previous models such as the cross sectional area and volume, to enable comparison between models. Starting with the geometry of model B, the central inclusion is replaced by a sphere with the same volume as the corresponding ellipsoid and a flat crack occupies the same area as the removed ellipsoid with a thickness equal to 5% of the radius of the sphere. A study on the thickness of this crack was performed for 5% and 1% showing there is almost no impact of this value in the equivalent material parameters for the aspect ratios considered (0.35 and 0.75). This value has an important effect on the concentration of electric field at the crack tip but, since this effect is highly localized, it does not affect the equivalent material parameters. Thus a further study or consideration of the crack thickness is not considered in this paper. Hence, the volume of this model is equal to the ellipsoidal volume, but with a different distribution of the air volume. The objective is to show the impact of the crack through the cross sectional area of the crack. This area is perpendicular to the direction of the polarization electric field and its size is defined by the aspect ratio. The ellipsoids at the corners are replaced by spheres with the same volume as these ellipsoids. The geometry of this model is presented in Figure 4.

It is shown later that cracks and ellipsoidal inclusions have similar effects on the equivalent material parameters, reducing their values.

2.4. Polarization Modelling

In the polarization process, termed "poling", each of the ferroelectric domains are subjected to an electric field which aligns them in the same direction as the applied electric field. The polarization of each of the domains depends on its material properties and the direction of the electric field present on these elements. The electric field at each domain is affected by the geometry and permittivity values of the composite. The material chosen for the matrix is barium titanate ($BaTiO_3$) and air for the inclusions. The air is modelled as a material, with very low elastic modulus ($\left(s^E_{air}\right)^{-1} \approx 100$ Pa), in order to represent accurately the dielectric constant of air ($\epsilon^T/\epsilon_0 \simeq 1$).

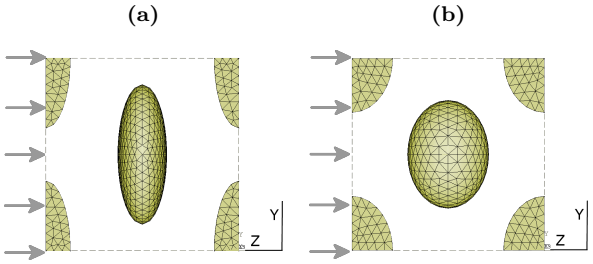

Figure 3: Geometry of the model B: Ellipsoidal model. The central inclusion is an ellipsoid with the minor axis aligned through the Z axis which is parallel to the polarization direction. The other two axes remains equal. Percentage of inclusions for the presented model is equal to 14%. a) Side view of model. $\tau = 0.35$. b) Side view of model. $\tau = 0.75$.

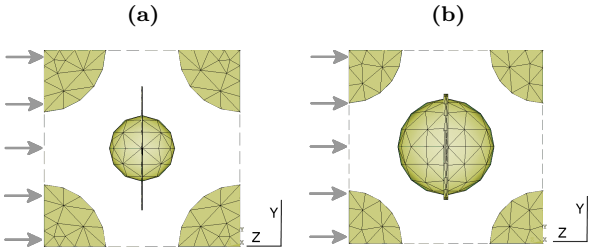

Figure 4: Geometry of the model C: Crack model. The central inclusion is an sphere with an area projected in the Z axis equivalent to the ellipsoidal central inclusion of the ellipsoidal model. Percentage of inclusions for the presented model equal to 15%. a) Side view of model. $\tau = 0.35$. b) Side view of model. $\tau = 0.75$.

Also, in order to obtain the electrical distribution inside the inclusion, the inclusion should be meshed.

The polarization state of the barium titanate has to be considered, being poled or un-poled. When the material is poled, the piezoelectric domains are aligned in the same direction. Then, the piezoelectric effect and transverse isotropic behaviour are exhibited. Its poled material properties are defined in Table 1. These material properties are taken from [39] for dense $BaTiO_3$, but the permittivity values have been changed since measurements have been undertaken of manufactured materials. In contrast, when the material is un-poled there is no piezoelectric effect ($d_{xx} = 0$) and the material is isotropic. The isotropic material properties are defined by two parameters s_{11} and ν_{12}. They are obtained following the approach presented in reference [40]. The permittivity values are obtained throughout averaging the poled values. The resistance of the un-poled material to be polarized is given by the coercive electric field parameter (E_{coer}) and it is equal to 0.5 MV/m [23].

The finite element model has been designed to be as representative as possible of the real fabrication process. The procedure is similar to the approach presented in reference [23] and starts by representing the geometry with all of the material in the un-poled state. An electric field is applied to the model by constraining the voltage at the top and bottom surfaces of the RVE to a value equal to the applied electric field (E_{app}) times the thickness of the RVE.

Table 1: Material properties of the poled and un-poled Barium Titanate ($BaTiO_3$). $\epsilon_0 = 8.854 \cdot 10^{-12}$ Farad/meter. Modified material properties based on Morgan Advanced Ceramic: Material Ceramic B. [39]

Coefficient	s^E_{11}	s^E_{22}	s^E_{33}	s^E_{12}	s^E_{13}	s^E_{44}	s^E_{55}	s^E_{66}	d_{31}	d_{32}	d_{33}	d_{15}	ϵ^T_{11}	ϵ^T_{22}	ϵ^T_{33}
Units	$p\text{Pa}^{-1}$	$p\text{Pa}^{-1}$	$p\text{Pa}^{-1}$	$p\text{Pa}^{-1}$	$p\text{Pa}^{-1}$	$p\text{Pa}^{-1}$	$p\text{Pa}^{-1}$	$p\text{Pa}^{-1}$	pC/N	pC/N	pC/N	pC/N	ϵ^T/ϵ_0	ϵ^T/ϵ_0	ϵ^T/ϵ_0
Poled	8.6	8.6	9.1	-2.6	-2.7	22.2	22.2	22.4	-50	-50	130	242	1600	1600	1500
Un-poled	8.45	8.45	8.45	-1.27	-1.27	9.72	9.72	9.72	0	0	0	0	1566	1566	1566

The influence of the polarization field is studied through a sweep of the applied electric field (E_{app}) between 90% and 110% of the coercive electric field (E_{coer}). After solving the model and obtaining the electric field in each of the elements, a loop through each one of the elements is performed to check if the electric field in that element is higher or lower than the coercive electric field. The orientation of that electric field is also obtained since the material element orientation of the poled material has to be aligned parallel to the electric field at the element centre. If the electric field in the element is higher than the coercive electric field, the element becomes polarized and the material properties of that element are replaced by the poled material properties oriented in the direction the electric field at the element. In any other case, the material of the element remains un-poled, which means it is remains as an isotropic material with zero piezoelectric coefficients. Since the polarization electric field is applied slowly, we neglect the dynamic effects in the charge application.

After the alignment of all elements, the model is solved again for the same applied poling field and its elements reoriented according to the conditions described above. Convergence is obtained when the increment of polarized FE elements between iterations is lower than 0.5% of the total number of elements in the model. Once the material polarization has reached convergence, the characterization procedure starts.

2.5. Material Characterization

Once the RVE material has reached polarization convergence, the characterization of the RVE starts. This process is explained in detail in reference [34] and it is briefly summarized here. Characterization is the name given to the procedure to obtain the equivalent electromechanical properties of a composite material knowing its individual material properties of each phase and using some assumptions. The equivalent electromechanical parameters are obtained using the *Hill Mandel condition* which can be summarized as the equivalent parameters, such as stresses or electric field, are approximately the averaged element parameters for the total volume of the RVE. A set of electromechanical deformations (strains, shears and voltage) are applied for each case using one possible deformation in each of the possible directions (x, y and z), namely U_x, U_y, U_z, τ_{xy}, τ_{yz}, τ_{xz}, E_x, E_y and E_z, giving a total of 9 cases. The model is solved for each of the cases to obtain stresses, strains, electrical displacements and electric fields in each element. After averaging the equivalent parameters , the corresponding equivalent elastic parameters $\overline{s}^E_{mn}$ are obtained by dividing the corresponding strain ($\overline{S}_m$) by the equivalent stress ($\overline{T}_n$). The piezoelectric material parameters $\overline{d}_{mn}$ are obtained diving the electric displacement ($\overline{D}_m$) by the equivalent stresses ($\overline{T}_n$), and the dielectric equivalent parameters ϵ^T_{mn} by dividing the corresponding electric displacement ($\overline{D}_m$) by the corresponding electric field ($\overline{E}_n$) [34].

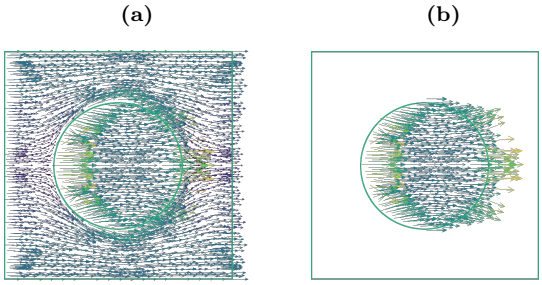

Figure 5: Polarization electric field and electric field distortion due to the inter-phase change. (a) Polarization electric field concept. In red the positive charges and in blue the negative charges distribution around the pore. (a) Electric field vector in the piezoelectric matrix. (b) Electric field vector in the air inclusion.

3. Results and discussion

3.1. Electric field distribution around a single inclusion

The polarization electric field decreases the magnitude of the applied electric field in the vicinity of the inclusion. In addition, the interface between inclusion and matrix provokes a change in the direction of the electric field, similar to optical refraction. This change of direction depends on the relative permittivity of the materials and the angle of incidence to the surface of the inclusion. The change in direction follows the Snell's rule with velocity replaced with permittivity $\sin\theta_1\epsilon_1 = \sin\theta_2\epsilon_2$ [41]. Where θ_1 is the angle of the incident electric field and θ_2 is the refracted electric field angle. The subindex 1 and 2 refer to the matrix and the inclusion respectively. From this equation, the electric field distortion can be obtained, as shown in Figures 5a and 5b. The distortion in the electric field direction is crucial, because it concentrates the electric field in specific places and decreases it in others.

Using the presented model, the effect of the polarization and the pore shape on the piezoelectric and dielectric coefficients are studied. Firstly, the electric field around an spherical inclusion inside a fully polarized material is studied. The presence of inclusions alters the electrical field distribution as Figure 6 shows. In Figure 6b, the normalized electric field in the matrix is clustered around the

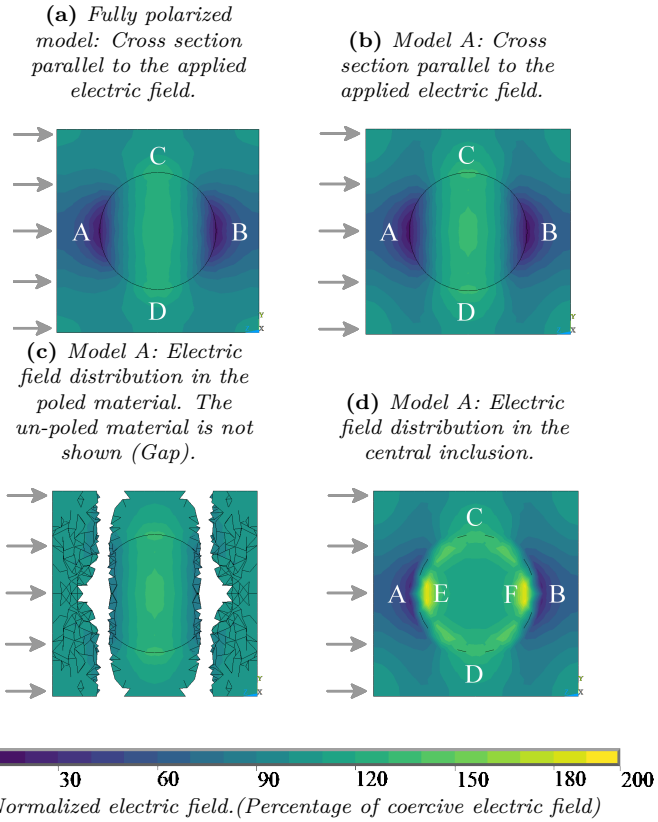

Figure 6: Normalized total electric field distribution with respect to the coercive field (100%) inside a fully polarized piezoelectric matrix material ((a)) and a partially polarized matrix ((b) (c) and (d)). The applied electric field is represented by grey arrows and it is equal to the coercive field. The porosity percentage is 20%.

top and bottom hemispheres (C and D), which are aligned perpendicular to the polarization electric field direction. In these zones, the electric field is up to 6 times higher than at the right and left hemispheres (poles A and B), where a weakened electric field is present. It should be noted that, although weakened, the electric field at the poles A and B has the same sign as at the poles C and D. Therefore, after increasing the electric field far enough, the poles A and B will polarized. However, in most of the cases these zones remain un-poled after the polarization process due to insufficient electric field to align the ferroelectric domains. Since these zones are not poled, they do not contribute to the effective material coefficients, which therefore become lower. The clustering of the electric field in the poles C and D and its corresponding weakening in the poles A and D leads to an accumulation of poled domains as layers perpendicular to the electric field, as Figure 6c shows. This layering of the material should not affect the dielectric coefficients, since the dielectric coefficient is similar for poled and un-poled material.

Finally the normalized electric field distribution inside the inclusions is presented in Figure 6d. In this figure, there are two high electric field clusters at the poles aligned with the electric field (poles E and F inside the ellipsoid). This is due to the change in phase, the different permittivity and the curvature of the inclusion which focus the incident electric field at the mentioned poles, following the Snell's law. This can be seen clearly in Figure 5b where the electric field penetrates the inclusion perpendicular to the surface in the left hemisphere concentrating at the pole E. A similar concentration happens at the pole F because of the inclusion curvature. These poles pair with the poles A and B in the matrix however the matrix counterpart has lower electric field magnitude.

3.2. Spherical model discussion

Firstly, the analysis of model A is presented in Figure 7. The model results are compared with the experimental data and the fully polarized model, in order to validate the approach. The experimental results correspond to samples which were manufactured using the BURPS method and the data is published in references [12, 22]. The pores on these samples are randomly distributed, therefore the poling behaviour of each sample might be different despite of being poled in the same way. In addition, the cracks presents uncertainty which increase the scattering of the samples. Different material coefficients show different trends, but all of them decrease when the porosity increases. The piezoelectric coefficient d_{31} shows an important decrease in magnitude, especially for porosity percentages up to 20% as Figure 7 shows. For higher percentages, the reduction is still present but at a lower rate. In contrast, the d_{33} coefficient shows a reduction for percentages lower than 15% but then remains almost constant for the rest of the measured range. Overall, the reduction in the coefficient d_{33} is lower than for d_{31}. The dielectric coefficient ϵ_{33}^T shows an almost linear dependency with respect to the porosity. The model 0 is also included in this comparison. The equivalent coefficients of this model show a decreasing trend as the experimental values, but these results are far from the experimental results, since it does not account for the polarization. An exception is the dielectric coefficient ϵ_{33}^T which presents an excellent match with the experimental results, showing a very strong correlation with the percentage of inclusions. Since all the domains exhibit the piezoelectric effect, and they are aligned in the same direction, the values of this model represent the theoretical maximum for the selected material parameters. Note that the fully polarized model represents an ideal model and, in practice, it is difficult to manufacture in laboratory due to the disturbance in the electric field due to the presence of inclusions, among other factors such us imperfections, contamination of the mixture, etc. Increasing the polarization field helps the experimental results to approach the theoretical maximum, but the risk of electrical breakdown increases too.

The results for the model A are presented in Figure 7. In this figure, the applied electric field is given by different dashed coloured lines and ranges from 90% to 110% of the coercive field. As expected, when a larger electric field is applied, more elements are polarized and therefore the equivalent material parameters tend to approximate

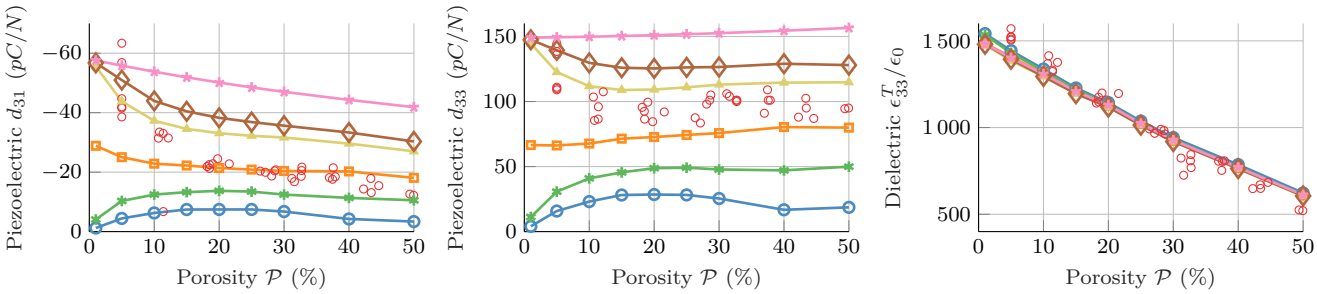

Figure 7: Results of the spherical model (Model A) for different values of applied electric field, aspect ratio and percentages of inclusions. The applied electrical field corresponds to 90% (—o—), 95% (—*—), 100% (—□—), 105% (—△—) and 110% (—◇—) of the coercive field. The experimental values (○) and the results of the fully polarized model (—*—) are also represented.

the fully polarized model. It can be seen also that after 105% increasing the applied electric field does not lead to a significant increment in the number of polarized elements. This is due to the saturation of the poles formed around the inclusions. With increasing applied electric field, the poles C and D keep increasing their electric field, but the elements at those poles are already polarized, and hence only the domains located at poles A and B can be polarized. The model predicts that about 98.5% of all piezoelectric domains become polarized when the applied electric field is double the coercive field, reaching approximately (99%) the fully polarized model values for the piezoelectric coefficient d_{33} and ϵ_{33}^T. When applying two times the coercive field, the applied electric field in some parts of the RVE almost reaches the electric field breakdown (E_{bd}) predicted by Neusel and Schneider [42] which is around $10^1 - 10^2$ MV/m for $BaTiO_3$ depending on the thickness and permittivity of the sample. Therefore, in practice, it is not possible to reach fully polarized model values by increasing the applied electric field, because of the electrical breakdown risk. To avoid this breakdown, it is important to know the applied electric field as well as its distribution. It should be noted that the dielectric breakdown strength depends on the thickness of the pellet [28, 42, 46], in addition on the porosity, and so the quoted value might not be the most appropriate in our case.

The change in the piezoelectric coefficient d_{33} in model A is predicted correctly, obtaining similar trends with respect to the experimental values. Between 10% and 50% of porosity, the values of d_{33} remain relatively constant, as the experiment and model show. The experimental values are close to the values given by the 105% of the coercive field, and they are always between 100% and 110% of the coercive ratio. The evolution of the coefficient d_{33} might be the result of the balancing of two factors, first the porosity which decreases the piezoelectric coefficients, and second, the concentration of electric field, which increases them. When the piezoelectric material is removed due to porosity, the electric field concentrates into the remaining ceramic material. For high porosity samples the amount of piezoelectric material is severely reduced, and thus all of the electric field clusters at very small volumes, which become polarized, increasing the piezoelectric coefficients. The authors believe that around 10% porosity the polarization due to the electric field concentration reaches a significant value with respect to the porosity, being able to change the rate of the decrease in the piezoelectric coefficients. A different trend is shown for the piezoelectric coefficient d_{31} which does not represent accurately the material behaviour for porosity percentages higher than 10%. The model shows a slow but constant decrease of the coefficient for the given range of porosities. However, experimental results show a more stepped change. The authors believe this decrease is due to the sphere inclusion which bends the electric field making it parallel to the inclusion surface. This parallel orientation is replicated by the polarized elements, giving a symmetry of the electric field with respect to a virtual axis parallel to the applied electric field as Figure 1a shows. This global symmetry in the RVE generates opposite electric fields in the perpendicular direction to the applied electric field which is related to the piezoelectric coefficient d_{31}. Given the infinite periodicity of the material properties (periodic boundary conditions), these electric fields cancel each other and hence the corresponding piezoelectric coefficient d_{31} decreases. The dielectric coefficient shows minor changes with respect to the applied electric field. This is a logical conclusion, since the dielectric properties do not change that much between polarized and un-polarized material (1500-1600 ϵ_s/ϵ_0 in the polarized material vs 1556 ϵ_s/ϵ_0 for the un-poled material). Later, in the discussion of the model B, it is shown that the aspect ratio has little effect on the values of the dielectric coefficient. Model A presents a good approximation for some important material coefficients such as the piezoelectric coefficient d_{33} and the dielectric coefficient ϵ_{33}^T, but it does not predict accurately the evolution of the coefficient d_{31} for increasing porosity after 10%.

3.3. Ellipsoidal model discussion

Firstly, the distribution of the electric field is studied in Figure 8 where the electric field of the sphere and the ellipsoidal models are compared, for two possible configurations. The applied electric field is equal to the coercive field or for the fully aligned and polarized model. For high

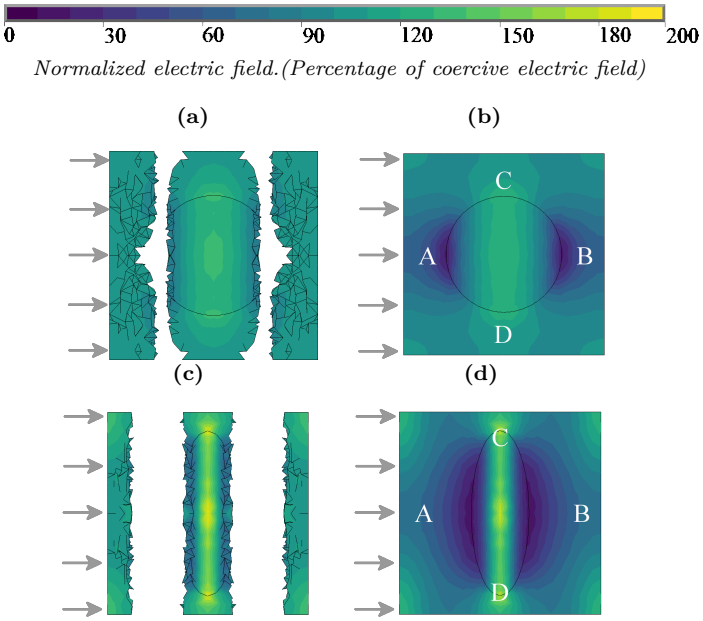

Figure 8: Comparison of electric field distribution for sphere model (upper figures) against high aspect ratio model (lower figures). Two different electrical configurations are displayed: applied electric field equal to coercive field (left) and fully polarized and aligned model (right). In the figures at the left, the unpoled domains are not plotted (gaps).

aspect ratio models, the electric field concentrates at the poles C and D. This is an effect of the repulsion between electrical charges, which concentrates electrons (and electric field) on high curvature areas and the electric field refraction. It is also true that the amount of volume affected by these poles is reduced as Figure 8 shows. In contrast, the poles A and B, which are unpoled, increase the amount of influenced volume. In the case of the fully polarized examples, it can be seen that the gradient of the electric field is much higher inside the inclusion. The electric field concentrates into the inclusion where it reaches electric fields around 180% of the applied electric field, and up to 10 times the electric field in the matrix. When the applied electric field is equal to the coercive field, it can be seen that due to the concentration of electric field in the inclusion, important amounts of ferroelectric domains remain unpoled, forming a clear sandwich structure composed of poled and unpoled material. It can be concluded then that the aspect ratio increases the charge density at the poles C and D, and reduces its affected volume. The electric field is concentrated at those poles, reducing its presence in the rest of the RVE. These high concentrations of electric field are prone to electrical breakdown. Under the same applied electric field the ellipsoid models give a lower number of polarized elements, and thus, lower piezoelectric coefficients. The results of model B are presented in Figure 9 for different values of aspect ratio, applied electric field and porosity. The aspect ratio values are 1, 0.75, 0.50 and 0.35 and they present a progressive change between spherical inclusion shape (aspect ratio equal to 1) and the extreme case of a flat crack (aspect ratio equal to 0). They aim to study the pore anisotropy introduced in the Introduction section. For comparison purposes, the sphere model is included too. To avoid geometry overlapping the maximum percentage of inclusions is limited to 35% for aspect ratio equal to 0.35, and to 50% for the rest of the cases. This model shows an important decrease in the piezoelectric coefficients when the porosity and aspect ratio increase. High aspect ratio models are related to very low piezoelectric values, for example, at 30% porosity the model with applied electrical field equal to 110% of the coercive field and aspect ratio equal to 0.35 obtains similar results to the models with 90% of the coercive field applied. This can be regarded as an increment of the unpoled material which is related to the electrical field distribution as shown in Figures 6 and 8. However, under a low applied electrical field (90%), higher aspect ratio yields higher piezoelectric coefficients due to the higher electrical field at the poles C and D. This trend is reversed for medium-high applied electrical field. The ellipsoidal model presents a general decrease in all the material coefficients for increasing aspect ratio at medium-high applied electric fields. The dielectric coefficient seems to be not much affected by the applied polarization field, as has been stated before. The aspect ratio impact on this coefficient is moderate, supposing a decrease about 30% of the coefficient value with respect to the sphere model for the model with aspect ratio equal to 0.35 and porosity equal to 30%. The piezoelectric coefficient d_{33} gives similar behaviour to the sphere model, with a more important decrease of the parameter at low porosity percentages and high aspect ratio. For an applied electric field equal to the coercive field, the aspect ratio is not a dominant parameter, and shows little effect for aspect ratios between to 0.35 or 0.75. For low applied electric field, the aspect ratio produces an increment of the piezoelectric coefficient, specially for high porosity percentages. A similar trend can be shown in the piezoelectric coefficient d_{31}, where aspect ratio gives a more rapid reduction of the parameter compared to the sphere model. At low applied electric fields, the aspect ratio is shadowed by the lack of polarized material hence has a negligible effect. Aspect ratio values lower than 0.35 might decrease the dielectric coefficient even more which already shows a good agreement between the experimental results and model A. Therefore, the authors believe that there is no need to model lower aspect ratio model than the current ones.

3.4. Crack model discussion

The electric field distribution of model C is detailed in Figure 10. In this figure, the normalized electric field with respect to the coercive field is presented for the poled material and for two aspect ratio values: 0.35 and 0.75. The applied electric field is equal to the coercive field. In the matrix, it can be seen that the electric field concentrates around the crack, reaching values up to 320% of the applied field. Inside the inclusion and the crack, the

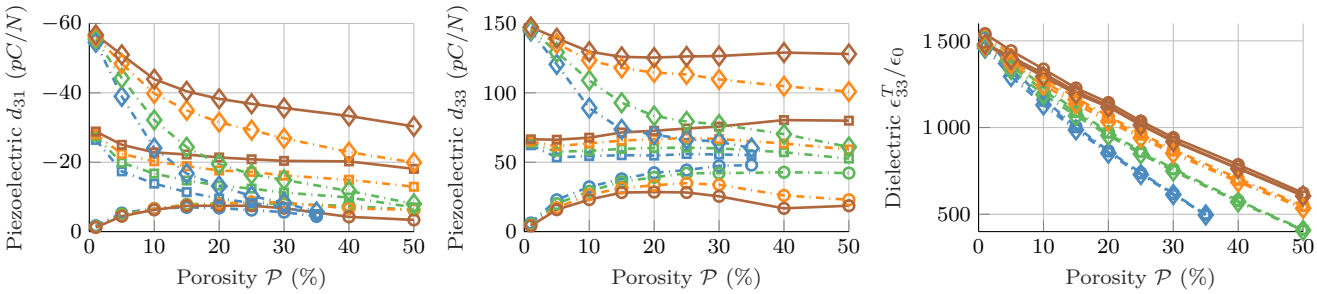

Figure 9: Results of the ellipsoidal model (Model B) for different values of applied electric field, aspect ratio and percentages of inclusions (axis X). The applied electrical field is represented with shapes: ○, □ and ◊ for applied electrical field equal to 90%, 100% and 110% of the coercive field respectively. The aspect ratio is represented with colours: blue, green, orange and red for values equal to 0.35, 0.5, 0.75 and 1 (spheric) respectively.

electric field reaches values up to 430% and 1800% of the coercive field for the 0.75 and 0.35 aspect ratio models respectively. The electric field decays rapidly with distance from the crack. As with the ellipsoidal model, the inclusions and crack absorb an important part of the electric field.

The model results are presented in Figure 11, for ellipsoidal ratios equal to 0.35, 0.5 and 0.75 respectively. In addition and for comparison purposes, the sphere model is included too. The results show almost identical trends with respect to the sphere model and the ellipsoidal model, but with higher piezoelectric values compared to the ellipsoids. The crack model gives similar dielectric coefficients to the sphere model, as expected, since the porosity is the same for both. However, experimental results have shown that the dielectric measurements are severely affected by the presence of cracks [26]. The important decreases in the experimental measurements might be due to the incomplete electric field transfer across the material because of the presence of cracks. Since our model is linear, the contribution of the cracks to the electric field transfer is assumed by the rest of the material, leading to a small impact on the dielectric properties and similar results to the spherical model. For the piezoelectric values, the crack model gives lower magnitudes than the sphere model, but higher than the ellipsoidal model. The coefficient d_{31} shows a continuously decrease in its magnitude, as shown by the experimental values presented previously in Figure 7. However, the crack model for high aspect ratio values lack the constant behaviour exhibited by the piezoelectric coefficient d_{33} for porosities between 10-50% shown by the experimental data and the sphere model.

This model gives a higher impact at high porosities, which is when the cracks might take more relevance. However this model does not show much change in the dielectric properties. This might be due to its small ratio cross section/porosity. It has been shown that the presence of cracks decreases the dielectric coefficient [7] and also that the cracks, especially at high porosity percentages, might expand across many pores [26]. This situation is not reflected in this paper. This model represents a first approximation to cracks modelling and it should be improved by including more accurate description of the geometry and fracture mechanisms. These mechanisms might be crucial in the characterization of highly fractured materials.

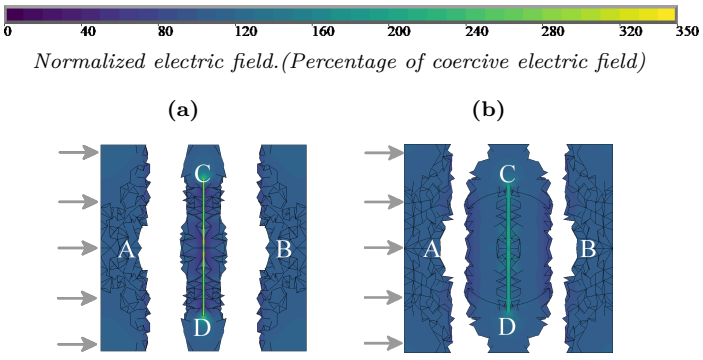

Figure 10: Comparison of electric field distribution for model C for two different aspect ratio values: 0.35 (left) and 0.75 (right). The applied electric field is equal to the coercive field. The un-poled domains are not plotted (gaps).

4. Conclusions

A detailed study has been performed on how the polarization electric field and the geometry of the inclusions affect the piezoelectric and dielectric coefficients of porous piezoelectric ceramics. Common inclusion shapes have been studied, namely spherical, ellipsoidal and ellipsoidal with a crack. Different aspect ratios and applied electric fields have been considered. The main conclusions are summarized as:

I High values of the applied polarization field might lead to high values of the equivalent parameters. However, there is a limit in the applied electric field due to electric breakdown because of electric field concentration at the poles.

II Important regions of the material are not polarized because of the presence of inclusions and their effect on the electric field.

III The electric field is concentrated around the poles of the inclusions due to refraction of the electric field. In

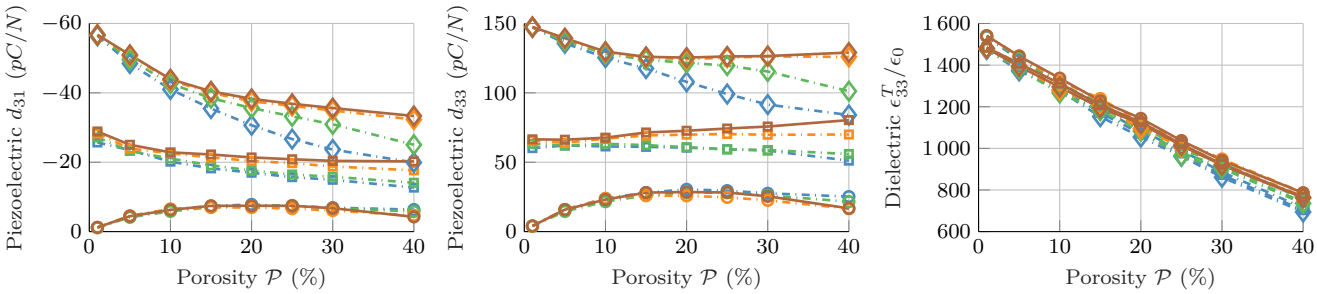

Figure 11: Results of the crack model (Model C) for different values of applied electric field, aspect ratio and percentage of inclusions (axis X). The applied electric field is represented with shapes: ○, □ and ◊ for applied electric field equal to 90%, 100% and 110% of the coercive field respectively. The aspect ratio is represented with colours: blue, green, orange and red for aspect ratio equal to 0.35, 0.5, 0.75 and 1 respectively.

the case of high aspect ratio models, the concentration of the electric field can reach values up to 200% of the coercive field at the high curvature poles. In the crack model, the maximum electric field concentration is found at the crack tip.

IV The symmetry in the electric field distribution with respect to the polarization axis is responsible for the important decrease in the piezoelectric coefficient d_{31}. Increasing the porosity, increases the amount of electric field distortion in the opposite directions and hence, decreases the equivalent parameters.

V The quasi-constant values of the coefficient d_{33} might be due to the progressive polarization of the domains located at the poles aligned with the polarization field (poles A and B). Increasing the porosity, also reduces the amount of volume where the electric field can flow, and hence the polarization of the piezoelectric domains increases. Thus because of the counterbalance between polarization and porosity, d_{33} remains relatively constant.

VI The model predicts that the dielectric coefficient might not be affected by the applied electric field. This parameter presents an almost linear correlation with the porosity percentage. However the aspect ratio seems to affect this material parameter for the geometries evaluated. In the presence of cracks, the cross section might have an important effect on the dielectric coefficient, but more accurate models are needed.

VII It has been shown that there is a strong interplay between ferro-elastic effects (switching with stress) and polarisation, leading to the formation of complex domain patterns in materials with complex stress fields [16]. The combination of complex distributions of both electric field (due to a permittivity contrast) and stress (due to a stiffness contrast) in porous ferroelectric materials may provide scope for further tailoring polarisation and properties.

VIII When the inclusion shape is accounted for during the modelling of the polarization process, the predicted piezoelectric coefficients are able to closely match the experimental values.

IX Future work should aim to model higher number of inclusions in order to account for effects such as distribution of porosity or clustering [6, 23]. Also, more representative geometry and material properties should be used in order to capture the material properties of structures with cracks. In addition, there is an interest to extend this approach to model material manufactured using other processes such as freeze-casting where the pore shape is closer to cylindrical or conical [48, 49].

Acknowledgement

The authors acknowledge the financial support from the Sêr Cymru National Research Network and Swansea University through a Postgraduate Scholarship NRN-103.

References

[1] S. R. Anton, H. A. Sodano, A review of power harvesting using piezoelectric materials (2003–2006), Smart materials and Structures 16 (3) (2007) R1.

[2] H. A. Sodano, D. J. Inman, G. Park, A review of power harvesting from vibration using piezoelectric materials, Shock and Vibration Digest 36 (3) (2004) 197–206.

[3] G. Martínez-Ayuso, M. I. Friswell, S. Adhikari, H. H. Khodaparast, C. A. Featherston, Porous piezoelectric materials for energy harvesting, in: International Conference on Noise and Vibration Engineering, 2016.

[4] R. Ramesh, H. Kara, C. Bowen, Characteristics of piezoceramic and 3–3 piezocomposite hydrophones evaluated by finite element modelling, Computational Materials Science 30 (3-4) (2004) 397–403.

[5] R. Ramesh, H. Kara, C. Bowen, Finite element modelling of dense and porous piezoceramic disc hydrophones, Ultrasonics 43 (3) (2005) 173–181.

[6] J. Roscow, R. Lewis, J. Taylor, C. Bowen, Modelling and fabrication of porous sandwich layer barium titanate with improved piezoelectric energy harvesting figures of merit, Acta Materialia 1359-6454.

[7] J. Roscow, Y. Zhang, J. Taylor, C. Bowen, Porous ferroelectrics for energy harvesting applications, The European Physical Journal Special Topics 224 (14-15) (2015) 2949–2966.

[8] R. Guo, C.-A. Wang, A. Yang, J. Fu, Enhanced piezoelectric property of porous lead zirconate titanate ceramics with one dimensional ordered pore structure, Journal of Applied Physics 108 (12) (2010) 124112.

[9] G. Martínez-Ayuso, H. H. Khodaparast, Y. Zhang, C. Bowen, M. Friswell, A. Shaw, H. Madinei, Model Validation of a Porous Piezoelectric Energy Harvester Using Vibration Test Data, Vibration 10.3390/vibration1010010.

[10] Y.-Y. Yu, C.-L. Liu, Y.-C. Chen, Y.-C. Chiu, W.-C. Chen, Tunable dielectric constant of polyimide–barium titanate nanocomposite materials as the gate dielectrics for organic thin film transistor applications, RSC Advances 4 (107) (2014) 62132–62139.

[11] P. Padmini, T. Taylor, M. Lefevre, A. Nagra, R. York, J. Speck, Realization of high tunability barium strontium titanate thin films by rf magnetron sputtering, Applied Physics Letters 75 (20) (1999) 3186–3188.

[12] J. I. Roscow, J. Taylor, C. R. Bowen, Manufacture and characterization of porous ferroelectrics for piezoelectric energy harvesting applications, Ferroelectrics 498 (1) (2016) 40–46.

[13] A. Chaipanich, N. Jaitanong, Effect of polarization on the microstructure and piezoelectric properties of PZT-cement composites, in: Advanced Materials Research, vol. 55, Trans Tech Publ, 381–384, 2008.

[14] Y. Zhang, J. Roscow, R. Lewis, H. Khanbareh, V. Y. Topolov, M. Xie, C. R. Bowen, Understanding the effect of porosity on the polarisation-field response of ferroelectric materials, Acta Materialia https://doi.org/10.1016/j.actamat.2018.05.007.

[15] H. Fu, R. E. Cohen, Polarization rotation mechanism for ultrahigh electromechanical response in single-crystal piezoelectrics, Nature 403 (6767) (2000) 281.

[16] E. K. Salje, S. Li, M. Stengel, P. Gumbsch, X. Ding, Flexoelectricity and the polarity of complex ferroelastic twin patterns, Physical Review B 10.1103/PhysRevB.94.024114.

[17] D. A. Kleinman, Nonlinear Dielectric Polarization in Optical Media, Phys. Rev. 10.1103/PhysRev.126.1977.

[18] L. Padurariu, L. Curecheriu, C. Galassi, L. Mitoseriu, Tailoring non-linear dielectric properties by local field engineering in anisotropic porous ferroelectric structures, Applied Physics Letters 100 (25) (2012) 252905.

[19] R. Khachaturyan, S. Zhukov, J. Schultheiß, C. Galassi, C. Reimuth, J. Koruza, H. von Seggern, Y. Genenko, Polarization-switching dynamics in bulk ferroelectrics with isometric and oriented anisometric pores, Journal of Physics D: Applied Physics 50 (4) (2016) 045303.

[20] C. Galassi, Processing of porous ceramics: Piezoelectric materials, Journal of the European Ceramic Society 26 (14) (2006) 2951–2958.

[21] H. Zhang, J.-F. Li, B.-P. Zhang, Microstructure and electrical properties of porous PZT ceramics derived from different pore-forming agents, Acta Materialia 55 (1) (2007) 171–181.

[22] J. I. Roscow, V. Y. Topolov, C. R. Bowen, J. Taylor, A. E. Panich, Understanding the peculiarities of the piezoelectric effect in macro-porous $BaTiO_3$, Science and Technology of Advanced Materials 17 (1) (2016) 769–776.

[23] R. W. Lewis, A. C. Dent, R. Stevens, C. R. Bowen, Microstructural modelling of the polarization and properties of porous ferroelectrics, Smart Materials and Structures 20 (8) (2011) 085002.

[24] R. Stanculescu, C. E. Ciomaga, L. Padurariu, P. Galizia, N. Horchidan, C. Capiani, C. Galassi, L. Mitoseriu, Study of the role of porosity on the functional properties of (Ba, Sr) TiO3 ceramics, Journal of Alloys and Compounds 643 (2015) 79–87.

[25] T. Zeng, X. Dong, C. Mao, Z. Zhou, H. Yang, Effects of pore shape and porosity on the properties of porous PZT 95/5 ceramics, Journal of the European Ceramic Society 27 (4) (2007) 2025–2029.

[26] C. Bowen, A. Perry, A. Lewis, H. Kara, Processing and properties of porous piezoelectric materials with high hydrostatic figures of merit, Journal of the European Ceramic Society 24 (2) (2004) 541–545.

[27] H. Kara, R. Ramesh, R. Stevens, C. R. Bowen, Porous PZT ceramics for receiving transducers, IEEE transactions on ultrasonics, ferroelectrics, and frequency control 50 (3) (2003) 289–296.

[28] R. Gerson, T. C. Marshall, Dielectric Breakdown of Porous Ceramics, Journal of Applied Physics 30 (11) (1959) 1650–1653.

[29] J.-F. Li, K. Takagi, M. Ono, W. Pan, R. Watanabe, A. Almajid, M. Taya, Fabrication and evaluation of porous piezoelectric ceramics and porosity–graded piezoelectric actuators, Journal of the American Ceramic Society 10.1111/j.1151-2916.2003.tb03430.x.

[30] R. Kar-Gupta, T. Venkatesh, Electromechanical response of porous piezoelectric materials, Acta Materialia 54 (15) (2006) 4063–4078.

[31] K. Challagulla, T. Venkatesh, Electromechanical response of piezoelectric foams, Acta Materialia 60 (5) (2012) 2111–2127.

[32] P. W. Bosse, K. S. Challagulla, T. Venkatesh, Effects of foam shape and porosity aspect ratio on the electromechanical properties of 3-3 piezoelectric foams, Acta Materialia 60 (19) (2012) 6464–6475.

[33] S. Iyer, T. Venkatesh, Electromechanical response of porous piezoelectric materials: Effects of porosity connectivity, Applied Physics Letters 97 (7) (2010) 072904.

[34] G. Martínez-Ayuso, M. I. Friswell, S. Adhikari, H. H. Khodaparast, H. Berger, Homogenization of porous piezoelectric materials, International Journal of Solids and Structures 113 (2017) 218–229.

[35] R. . ANSYS® Academic Research Mechanical, Theory reference for the Mechanical APDL and Mechanical Applications„ ANSYS, Inc, release 18.1 edn., ????

[36] P. Suquet, Local and global aspects in the mathematical theory of plasticity, Plasticity Today: Modelling, Methods and Applications (1985) 279–310.

[37] K. Terada, M. Hori, T. Kyoya, N. Kikuchi, Simulation of the multi-scale convergence in computational homogenization approaches, International Journal of Solids and Structures 37 (16) (2000) 2285–2311.

[38] E. Mercadelli, A. Sanson, C. Galassi, Porous piezoelectric ceramics, in: Piezoelectric ceramics, InTech, 2010.

[39] D. Berlincourt, H. Krueger, C. Near, Properties of Morgan electro ceramic ceramics, Morgan Electro Ceramics, Report No. TP-226 .

[40] C. R. Bowen, A. C. Dent, R. Stevens, M. G. Cain, A. Avent, A new method to determine the un-poled elastic properties of ferroelectric materials, Science and Technology of Advanced Materials 18 (1) (2017) 264–272.

[41] N. Jonassen, Electrostatics, Springer Science & Business Media, 2013.

[42] C. Neusel, G. A. Schneider, Size-dependence of the dielectric breakdown strength from nano-to millimeter scale, Journal of the Mechanics and Physics of Solids 63 (2014) 201–213.

[43] J.-c. Luo, P.-z. Li, The electric breakdown problem in piezoelectric material containing a semi-permeable crack, in: Piezoelectricity, Acoustic Waves, and Device Applications (SPAWDA), 2014 Symposium on, IEEE, 222–225, 2014.

[44] N. Klein, Electrical breakdown in solids, in: Advances in electronics and electron physics, vol. 26, Elsevier, 309–424, 1969.

[45] K. D. Schomann, Electric breakdown of barium titanate: A model, Applied physics 6 (1) (1975) 89–92.

[46] A. Branwood, O. Hughes, J. Hurd, R. Tredgold, Evidence for space charge conduction in barium titanate single crystals, Proceedings of the Physical Society 79 (6) (1962) 1161.

[47] I. Sevostianov, M. Kachanov, Connections between elastic and conductive properties of heterogeneous materials, in: Advances in applied mechanics, vol. 42, Elsevier, 69–252, 2009.

[48] Y. Zhang, L. Chen, J. Zeng, K. Zhou, D. Zhang, Aligned porous barium titanate/hydroxyapatite composites with high piezoelectric coefficients for bone tissue engineering, Materials Science and Engineering: C 39 (2014) 143–149.

[49] Y. Zhang, Y. Bao, D. Zhang, C. R. Bowen, Porous PZT ceramics with aligned pore channels for energy harvesting applications, Journal of the American Ceramic Society 98 (10) (2015) 2980–2983.